Aurora B Kinase Dependent Phosphorylation of Keratin 8 is required for Cytokinesis in Mammalian Cells of Epithelial Origin

Busra Harmanda[1], Oyku Kaya[1], Xenia Waide[1,2], Muhammed Haroon Qureshi[1], Alexey Nesvizhskii[3], Timothy J Mitchison[4], Nurhan Ozlu[1*]

[1] Department of Molecular Biology and Genetics, Koç University, 34450, Istanbul, Turkey
[2]Faculty of Chemistry and Biochemistry, Ruhr-Universität-Bochum, 44801 Bochum, Germany
[3] Department of Computational Medicine and Bioinformatics, University of Michigan, Ann Arbor, Michigan 48109, United States
[4] Department of Systems Biology, Harvard Medical School, Boston, MA, United States

*Correspondence and requests for materials should be addressed to NO (email: nozlu@ku.edu.tr)

Abstract

Keratins are the most diverse family of intermediate filaments and are expressed in most epithelial tissues and malignancies. They form highly stable polymers that need to be cut through during cytokinesis. Previous work suggested a role of phosphorylation, but keratin regulation during cell division is not understood in detail. Depletion of Keratin 8 in an epithelial cancer cell line (HeLa) caused chromosome segregation and cytokinesis defects. Aurora B kinase localization to midzones and cleavage furrows was reduced in Keratin 8 knockouts, suggesting that Keratin 8 helps scaffold Aurora B during cytokinesis. We mapped eleven Aurora B kinase sites in Keratin 8 that were associated with cell division. Keratin 8 S34 phosphorylation occurred specifically at the cleavage furrow and persisted at the midzone until the end of cytokinesis. Inhibition of Aurora B kinase or non-phosphorylatable Keratin 8 mutant prevented the disassembly of keratin bundles at the cleavage furrow, which blocked furrow ingression. Our data reveal a functional inter-dependency between Keratin 8 and Aurora B kinase in epithelial cells. Keratin 8 promotes the translocation of Aurora B to the midzone. Aurora B kinase then generates a local zone of Keratin phosphorylation which promotes keratin filament disassembly and allows the cleavage furrow to cut through the keratin network.

Keywords Keratin, cytokinesis, Aurora B Kinase, phosphorylation, Keratin solubility, cleavage furrow, epithelial origin

Introduction

Keratin filaments are a class of intermediate filaments that is abundant in epithelial cells where they provide mechanical integrity and poorly understood regulatory roles (Ku *et al*, 2004) . Keratin proteins are expressed in pairs that heterodimerize to generate polymerizing subunits, with different cell types expressing characteristic pairs (Karantza, 2011). Keratin 8/18 subunits are typically expressed in proliferating epithelial progenitor cells as well as many epithelial cancers and cancer-derived cell lines and are thus of particular relevance when considering the roles of keratins in cell division.

The most obvious functional concern in the biology of keratins during cell division is the need to remove them, in whole or part, to allow the successful execution of mitosis and cytokinesis. Keratin filament networks, which span the whole cytoplasm and connect between cells at desmosomes (Hatzfeld *et al*, 2017), have the potential to physically impede mitotic spindle assembly and cleavage furrow ingression. Early studies suggested the Keratin 8/18 network globally disassembles into non-filamentous aggregates at the onset of mitosis (Lane *et al*, 1992). Later work showed that in some epithelial cell types, keratin disassembly is spatially organized to generate a filament-free cage in which the mitotic spindle assembles (Rieder & Hard, 1990). Temporal and spatial control of intermediate filament organization during cell division is exerted by kinases that phosphorylate subunits and typically drive the monomer-filament system towards disassembly (Inaba *et al*, 2018). Control of vimentin polymerization by phosphorylation during cell division has been studied in depth, and it is known that Aurora-B kinase has an important regulatory role (Eriksson *et al*, 2004; Goto & Inagaki, 2007). Control of keratin organization during cell division has been much less studied, despite the importance of keratins in tissue biology and epithelial cancers. Keratins are heavily phosphorylated and their phosphorylation levels are enhanced during mitosis (Chou *et al*, 1993). Keratins are probably phosphorylated by multiple kinases during mitosis. Keratin 5/14 were reported to be phosphorylated by CDK1, Rho-kinase and Aurora B kinases during cell division (Inaba *et al.*, 2018).

Most studies portray intermediate filaments as potential blocks to cell division that must be removed. However, some studies showed that vimentin filaments promote spatially organized signaling during cell migration (Helfand *et al*, 2011; Prahlad *et al*, 1998). Vimentin is thought to serve as a scaffold that promotes the local activity of ERK kinase (Virtakoivu *et al*, 2015). It is possible that K8/18 filament contribute to the spatial organization of cell division in epithelial progenitors and cancers, for example by helping scaffold cell division kinases, but this hypothesis has to be systemically addressed.

Aurora B kinase acts in cell division as part of the Chromosomal Passenger Complex (CPC). During metaphase and anaphase CPC localizes to centromeres and the surface of chromosomes where it regulates chromosome condensation and helps correct errors in kinetochore-microtubule attachments (Carmena *et al*, 2012). At the onset of cytokinesis, it translocates to the spindle midzone where it promotes assembly and ingression of the cleavage furrow. Midzone-localized Aurora B also generates a phosphorylation gradient that helps to resolve segregation errors in between segregating chromosomes (Orr *et al*, 2021; Papini *et al*, 2021) and delays abscission when unsegregated chromosomes are trapped at the cleavage site (Chen & Doxsey, 2009; Steigemann & Gerlich, 2009).

In our previous phospho-proteomic studies, we found that phosphorylation of Keratin 8 and 18 were diminished after Aurora B kinase inhibitor treatment (Ozlu *et al*, 2010; Polat *et al*, 2015). In Xenopus laevis eggs, a model system for epithelial cell division, keratins are globally disassembled during mitosis, presumably by CDK1 activity (Bachant & Klymkowsky, 1996; Gard, 1999), and locally disassembled between microtubules asters during interphase by Aurora B kinase activity (Field *et al*, 2019).

In this study, we generated Keratin-8 knockout Hela cells and investigated Keratin-8 function during cell division. We showed that depletion of Keratin 8 reduced Aurora B kinase levels at the chromosomes and midzone and increased the rate of multinucleated cells. *In vitro* analysis revealed that Aurora-B phosphorylate eleven Keratin 8 sites. Aurora B kinase interacts with Keratin 8 in a phosphorylation and cell-cycle dependent manner. Aurora B-dependent Keratin 8 phosphorylation (K8 phosphoS34) decorates cleavage furrow and facilitates Keratin 8 disintegration during furrow ingression. Ectopic expression of non-phosphorylatable Keratin 8 dramatically increases cleavage furrow regression. We propose that interaction between Aurora B kinase and Keratin 8 have mutual effects: it helps translocation of Aurora B to the midzone and promotes Keratin disintegration during cleavage furrow ingression in epithelial cells and epithelial malignancies.

Results

Knock-out of Keratin-8 causes chromosome segregation and cytokinesis defects

To characterize the role of Keratin 8 during cell division we employed CRISPR/Cas9-mediated knockout of Keratin 8 in a standard epithelial cancer cell model, HeLa (K8 KO). Western blotting and immunofluorescence analyses confirmed the efficient knockout of Keratin 8 in K8 KO cells. In these assays non-targeting guide RNA expressing cells were used as a control **(Supplementary Figure 1A, B)**. K8 KO cells were viable and grew at a similar rate to controls. To detect possible cell division defects, we performed live-cell imaging in wild type (WT) and K8 KO cells expressing Histone 2B-mCherry. Strikingly, K8 KO cells exhibited frequent defects in chromosome congression visible as misaligned and lagging chromosomes. When Keratin 8 expression was replenished by exogenous K8-GFP expression (K8 KO+WT K8-GFP), the division proceeded without detectable defects **(Figure 1A, Videos S1-S3)**.

In K8 KO cells, we observed that after cleavage furrow ingression, occasionally abscission failed which led to multinucleated cells. To quantify cytokinesis defects, we immunostained HeLa cells with anti-tubulin antibodies and scored multinucleated cells **(Supplementary Figure 1C)**. K8 KO cells had a moderate but statistically significant increase in the fraction of multinucleated cells in comparison to the control **(Figure 1B, Supplementary Figure 1C)**. K8-GFP expression in K8 KO cells largely rescued the multinucleation phenotype and resulted in significant reduction in multinucleation rate (Figure 1B). To examine chromosome alignment during metaphase, we visualized DNA, and tubulin by immunofluorescence in WT, K8 KO and K8 KO+WT K8:GFP cells (**Figure 1C**). In K8 KO cells, there was a significant defect in the chromosome congression (48%) which is visible by the satellite DNAs around the metaphase chromosome. Re-expression of Keratin 8 corrected this defect **(Figure 1D)**. Next, we investigated the timing of cell division progression in K8 KO cells by live imaging and observed a significant delay in the completion of abscission (Supplementary Figure 1 D, F, **Videos S4-5**).

Defects in both metaphase chromosome alignment and cytokinesis abscission in K8 KO cells suggested that Keratin 8 might play a role in localizing or activating Aurora B kinase, which is involved in both processes (Steigemann *et al*, 2009). To test this hypothesis, we localized Aurora-B kinase in WT vs K8 KO cells, focusing especially on anaphase-telophase in cells that exhibited lagging chromosomes and chromosome bridges **(Figure 1E)**. Strikingly, we also observed that Aurora B levels of those defective cells at the cleavage furrow are low (**Figure 1E**). Aurora B localization in the K8 KO cells is quantified below (see Figure 5 C, E). Quantification of lagging and bridged chromosomes at anaphase revealed a significant increase in abnormal chromosome segregation in Keratin 8 KO cells **(Figure 1F)**.

Fixed immunofluorescence might not be reliable for the quantification of local Aurora B kinase concentrations. To measure the Aurora B levels in live cells, we co-expressed Aurora B-GFP and

Histone 2B-mCherry in WT vs K8 KO HeLa cells (**Figure 1G, Videos S6-S7**). Strikingly, we observed a significant decrease in the chromosomal and cleavage furrow localization of Aurora B (about two-fold of decrease in the chromosomal Aurora B-GFP intensity) in K8 KO cells (**Figure 1H, Supplementary Figure 1G).** Total Aurora B protein expression was not different in control versus K8 KO cells (Supplementary Figure 1H) suggesting that Aurora B cannot be properly targeted to the chromosomes and cleavage furrow in the absence of Keratin 8.

Aurora-B phosphorylates Keratin 8 during cell division

Our previous proteomic analysis suggested that Keratin 8 is phosphorylated by Aurora B kinase during cell division (Ozlu *et al.*, 2010). To test this, we performed an *in vitro* kinase assay followed by mass spectrometry analysis. We expressed the Keratin 8-GST fusion protein in bacteria and purified it using glutathione beads. Keratin 8-GST and active Aurora B complexed with a fragment of INCENP were incubated in a kinase reaction buffer in the presence of ATP. A parallel reaction that has only Keratin 8-GST but lacks Aurora B complex is performed as a control **(Figure 2A)**. The Aurora B dependent Keratin phosphorylations are quantified by monitoring Keratin 8 phosphopeptides and their non-phosphorylated counterparts by PRM (Parallel Reaction Monitoring) experiments using HF-Exactive Mass Spectrometry. Keratin 8 S34 phospho and nonphospho-forms are quantified in both -/+ Aurora B kinase set-up **(Figure 2B, Supplementary 2A-F)**. By this approach, we map the Aurora B kinase dependent Keratin 8 phosphosites in vitro. As a result S34, S37, S124, S330, S404 and S475 Keratin 8 residues were phosphorylated in the presence of Aurora B **(Figure 2C, Supplementary 2A-F)**. Previously in a global phosphoproteome study, we analyzed cell cycle dependent changes in Keratin phosphorylations and determined that S13, S34, S35, S36, S37, S39, S43, S44, S104, S258 phosphosites of Keratin 8 are up-regulated in mitosis or cytokinesis (Ozlu *et al.*, 2010).

Aurora B dependent Keratin 8 phosphorylation is required for cytokinesis

To analyze the role of Aurora-B dependent phosphorylation of Keratin 8, we decided to focus on S13, 34, 35, 36 and 37 which are in a highly phosphorylated region at the head domain **(Figure 2B-C)**. Our previous study also identified S13, S34 and S37 Keratin as cytokinesis selective phosphorylation sites whose levels were diminished when cells were treated with an Aurora inhibitor, VX680 (Ozlu *et al.*, 2010). To test the role of these phosphorylation sites in cell division, we expressed a 5XA mutant fused to GFP, where S13, 34, 35, 36 and 37 were mutated to alanine in K8 KO cells. We then quantified multinucleation, which provides a simple readout of cytokinesis failure (**Supplementary Figure 3A)**. In agreement with our previous observation, we observed a slight but significant increase in multinucleation in K8 KO cells compared to control ones which were rescued in K8 KO+WT K8:GFP expressing cells. In K8 KO + K8-5XA-GFP cells, the percentage of multinucleated cells dramatically increased **(Figure 3A, Supplementary Figure 3A)**. Next, we created S13, S34-35A K8; S13,S36-37A K8 and S13A K8 mutants separately and assessed their affect in cytokinesis. Western blotting analysis showed that total protein levels of all mutated K8 are comparable **(Supplementary Figure 3B)**. Among all three mutations, S13, S34-35A K8 caused the highest rate of multinucleation in K8 KO cells albeit it was not as high as in 5XA mutants (Figure 3A). This result shows that non-phosphorylatable Keratin-8 strongly perturbs cytokinesis and phosphorylation of S34 and S35 have higher impact on cytokinesis.

Next, we asked whether nonphosphorylatable Keratin 8 can rescue the chromosome congression phenotype of K8 KO cells. For this purpose, we performed immunostaining to visualize DNA and tubulin at metaphase in K8 KO cells expressing WT K8 or K8-5xA (**Supplementary Figure 3C**). In control metaphase cells, the chromosome congression defects were minimal (less than 10%) whereas we observed a significant increase in chromosome congression defects in K8 KO (around 70% of cells had misaligned chromosomes). This phenotype was largely rescued upon WT Keratin 8 expression. K8-5XA

expression in K8 KO cells still had severe chromosome congression defects albeit not as severe as in K8 KO cells **(Supplementary Figure 3D)**. Altogether, these data suggest that Keratin phosphorylation is essential for chromosome orientation and cytokinesis.

To gain more insight into the role of Aurora B dependent Keratin 8 phosphorylation in cytokinesis, we closely examined WT and phospho-mutant (S13, 34-37A) K8-GFP expressing cells. In WT K8-GFP expressing HeLa cells, Keratin 8 disappeared at the cleavage furrow of cytokinesis cells. Interestingly, 5XA K8-GFP expressing cells exhibited residual Keratin 8 at the cleavage furrow **(Figure 3B)**. WT K8 was cleared from a region a few microns wide around the ingressing furrow, while 5XA K8 intensity was almost uniform across the center of the cell. Quantification of WT and mutant Keratin 8 expressing cells supported significantly more Keratin 8 bundles at the cleavage furrow in 5XA Keratin 8-GFP expressing cells than WT ones (**Figure 3C).** To further elaborate on this finding, we performed live imaging of WT and S13,34-37A Keratin 8-GFP in K8 KO cells. WT and 5XA mutant K8- GFP had indistinguishable distribution in interphase and mitosis. In both cases at the onset of mitosis, keratins disintegrate probably through CDK1-dependent phosphorylation (Inaba *et al.*, 2018). However, during cytokinesis in contrast to WT, 5XA K8-GFP expressing cells had residual keratin bundles at the cleavage furrow **(Figure 3D).** Importantly, Keratin 8 bundles and bridges at the cleavage furrow resulted in cytokinesis failure and multinucleation in the 5XA K8-GFP expressing cell **(Figure 3D, Videos S8,S9)**.

These results suggest that Aurora B dependent phosphorylation of Keratin 8 is required for the dissolving of Keratin 8 filaments at the cleavage furrow. If this is the case, Aurora B inhibition should affect the Keratin 8 distribution similarly. To test this, we synchronized Hela cells at the mitosis by nocodazole and then released them to cytokinesis. Thirty minutes after the release, we treated the cells with Aurora B inhibitors (AZD1152 and VX680) for a further thirty minutes. We performed immunostaining in control and AZD1152/VX680 treated cells by using anti-Keratin 8 and anti-INCENP antibodies **(Figure 3E)**. Consistent with the results above, Keratin 8 persisted and in some cells formed large bundles at the cleavage furrow upon Aurora B inhibition whereas Keratin 8 disintegrated and was not visible at the midzone in control cells (**Figure 3E)**. Quantification of multiple control and AZD1152 or VX680 treated cells revealed more than two fold increase in the Keratin intensity at the cleavage furrow (**Figure 3F).** Live imaging of AZD1152 or VX680 treated cells also confirmed those results (**Supplementary Figure 3E, Videos S10-S12**). Strikingly we observed large bundles of Keratin filaments in Aurora B inhibitor treated cells. These results support that phosphorylation of Keratin 8 by Aurora B kinase is required for furrow ingression.

Phosphomimetic mutant of Keratin 8 leads to speckled Keratins

To further elaborate on the role of Aurora B dependent phosphorylation of Keratin 8, we attempted to create a phosphomimetic mutation of Keratin 8 and assess its behavior in cytokinesis. Our mutation analysis above suggested that phosphorylation of S34-S35 are critical for cytokinesis, thus we targeted those sites. Indeed, expression of S34-35D phosphomimetic mutation of K8 did not cause a significant number of multinucleation in K8 KO cells, the multinucleation rate was similar to the control cells **(Figure 3A)**.

Next, we examined the subcellular distribution of S34-35D K8 in mitotic cells by immunostaining. S34-35D K8-GFP expression in K8 KO cells revealed that the phosphomimetic mutant of K8 has rather different morphology **(Figure 4A, Videos 13-15)**. In contrast to 5XA mutant expressing K8 KO cells, where K8 often accumulates at the cleavage furrow, we did not observe keratin bundles in S34-35D K8-GFP expressing K8 KO cells. Interestingly, S34-35D mutation resulted in higher percentage of cells (> 80%) with speckled keratins throughout mitosis and cytokinesis. Thus, S34-35D mutation may facilitate structural changes in K8 and promote its solubility.

Aurora B-dependent Phosphorylation of Keratin 8 decorates cleavage furrow

Our data showed that Aurora B dependent phosphorylation of Keratin 8 is essential for successful cytokinesis. S34 is associated with Aurora B consensus motif, and our in vitro kinase assay showed that its phosphorylation is Aurora B dependent (Figure 2). To examine Aurora-B dependent spatial and temporal regulation of Keratin 8 phosphorylation during division, we raised custom phospho-specific antibodies against phospho-S34 Keratin. We initially confirmed the specificity of the antibody by immunostaining of K8 KO cells (**Supplementary Figure 4**). To image the subcellular localization of phosphorylated Keratin 8, unsynchronized HeLa cells were immunostained using anti-K8 and anti-Phospho S34 K8 antibodies. Although Keratin 8 decorated the inside of cells throughout the cell cycle, phospho S34 K8 was only detectable at the onset of anaphase, as chromosomes segregate it strongly localized at the contractile ring as the cleavage furrow ingress and persisted at the neighboring cortical part of newly divided daughter cells during abscission (**Figure 5A**). To confirm the phosphorylation of S34 K8 by Aurora B kinase in vivo, we treated cells with Aurora B kinase inhibitors AZD1152 or VX680 and examined Phospho S34 K8 levels. Notably, Aurora B kinase activity inhibition abolished the contractile ring localization of S34 Keratin 8 phosphorylation (**Figure 5B**). Phosphorylated S34 Keratin 8 absolutely disappeared both at anaphase and telophase cells upon Aurora B inhibition (**Figure 5C**). To test whether this phosphorylation pattern is conserved in Keratin expressing cells, in addition to HeLa cells, we also tested the localization of Phospho S34 K8 in an epithelial cell line, MCF7. Similar to the expression pattern in HeLa cells, Phospho S34 K8 was only detectable at the onset of anaphase and it was confined to the cleavage furrow until the end of cytokinesis (**Supplementary Figure 5A**). When MCF7 cells are treated with Aurora B inhibitors, phospho S34 staining is completely abolished (**Supplementary Figure 5B**). These results support the conservation of cytokinesis specific and Aurora B dependent phosphorylation of Keratin 8 in all Keratin 8 expressing cells.

Keratin 8 helps target Aurora B kinase during cell division

The findings above suggest temporal and spatial regulation of Keratin 8 phosphorylation by Aurora B kinase. To elaborate on the interaction between Keratin-8 and Aurora B, we tested whether Aurora B physically associates with Keratin-8 during cell division. For this, we employed Aurora B-GFP expressing cells where GFP tagged Aurora B is expressed under its own promoter using bacterial artificial chromosome (BAC) transgenomics in HeLa cells (Poser *et al*, 2008). We pulled down Aurora B-GFP from the cell extracts arrested in interphase and mitosis. Aurora B interacted with Keratin 8 in mitosis but not in the interphase **(Figure 6A, Supplementary Figure 6 A-C)**. In parallel, we performed GFP pulldown from WT K8-GFP and mutant (S13, 34-37A) K8-GFP expressing in K8 KO cells and empty GFP expressing K8 KO cells were used as a control **(Supplementary Figure 6 A-C)**. We observed that a small portion of Aurora B interacted with Keratin 8 in mitosis and cytokinesis cells but not in interphase. Importantly, only WT K8-GFP interacted with Aurora B but not the mutant (S13, 34-37A) K8 GFP **(Supplementary Figure 6 A-C)**. If the Aurora B and Keratin 8 interaction is phosphorylation dependent, we propose that inhibiting Aurora-B kinase activity would impair this interaction. Indeed, when Aurora-B GFP expressing mitotic cells are treated with AZD1152 the elutes of Aurora-B pull down do not have detectable Keratin-8 (**Supplementary Figure 6D)**. These findings suggest that Aurora B kinase dependent phosphorylation promotes Keratin 8- Aurora B interaction and it is confined to mitosis and cytokinesis stages.

Next, we tested whether Keratin-8 or its phosphorylated form plays roles in targeting Aurora B kinase to the chromosomes or cleavage furrow. Immunostaining of Aurora B in the control cells showed that Aurora B decorated the whole metaphase chromosomes. In agreement with our previous results, in K8 KO cells, chromosomal Aurora B localization is strongly perturbed which was replenished after Keratin 8-GFP expression in K8 KO cells (**Figure 5B, C**). However, S13A,34-37A Keratin 8 expression in the K8 KO background was not able to recruit Aurora B kinase to the metaphase chromosomes

(**Figure 5B, C**). Consistent with our previous result, Aurora B localization at the cleavage furrow was also disrupted in Keratin 8 knockout cells. Exogenous expression of WT Keratin 8 rescued Aurora B localization at the cleavage furrow (**Figure 5D, E**). Importantly, S13A, S34-37A Keratin 8-GFP expressing cells were not able to recruit Aurora B to the cleavage furrow (**Figure 5D, E**). The cleavage localization of Aurora B kinase was significantly compromised in phospho mutant expressing cells. Overall, these findings suggest that Keratin 8 targets Aurora B to the chromosome and cleavage furrow and Aurora B dependent phosphorylation of Keratin 8 specifically facilitates targeting of Aurora B kinase to the metaphase chromosomes and cleavage furrow in keratin expressing cells.

DISCUSSION

Intermediate filaments are the least studied elements of the cytoskeleton and have been largely ignored by the cell division research community. Yet, it has long been recognized that intermediate filaments must be dissolved, either locally or globally, for cytokinesis to succeed. Intermediate filament localization usually involves phosphorylation. Phosphorylation of nuclear lamins by CDK1 has long served as a paradigm for both intermediate filament and CDK1 biology (Dechat *et al*, 2010; Gerace & Blobel, 1980). Aurora B-dependent phosphorylation of vimentin is also a classic story for the role of spatially regulated kinase activity in cell division (Goto *et al*, 2003). However, very little is known about cell-cycle dependent organization of Keratin filaments. Here, we showed that cytokinesis-specific and Aurora B-dependent phosphorylation of Keratin 8 decorates the cleavage furrow, and it triggers the disintegration of Keratin bundles at the cleavage furrow (Figure 7).

It is well established that keratin filament reorganization is highly regulated by post-translational modifications and phosphorylation of keratin filaments increases its solubility and helps dissolve the keratin network (Chou *et al.*, 1993; Omary *et al*, 1998). In this study, we mapped eleven Aurora B-dependent phosphorylation sites in Keratin 8. Our work focused on one of the Aurora B-dependent phosphorylation sites, pS34 K8. Aurora B kinase phosphorylates Keratin 8 S34 at the onset of anaphase as a cleavage furrow begins to form. pS34 K8 decorates cleavage furrow and persists until the completion of furrow ingression. We propose that Aurora B-dependent phosphorylation disintegrates Keratins specifically at the cleavage furrow. By employing Aurora kinase inhibitors, Field et al. showed that the disassembly of keratin filaments between sister asters in *Xenopus egg* extracts requires Aurora B kinase activity (Field *et al.*, 2019). However, that study did not identify any phosphosites or test the role of non-phosphorylatable mutant keratin. Similarly, we observed that in human cells Aurora B inhibition and non-phosphorylatable Keratin 8 causes residual keratin bundles at the cleavage furrow. Previous work on the inhibition of cytokinesis by Aurora B inhibitors assumed that these drugs work by blocking signaling pathways leading to RhoA activation at the furrow cortex (Carmena *et al.*, 2012; David *et al*, 2012). Our results show that an additional factor is the blockade of furrow ingression by keratin filaments when they cannot be phosphorylated by Aurora B.

The phospho-S34 Keratin antibody generated in this study provides a readout of the spatial extent of Aurora B kinase activity as well as a biomarker for cytokinesis. Spatial regulation of Aurora B kinase was previously demonstrated using a live cell FRET biosensor (Fuller et al., 2008; Liu et al., 2009), which has the advantage of temporal readout, but our antibody is technically simpler to implement and useful for fixed samples. Multiple anti-mitotic phospho-antibodies are used to detect mitotic cells including phospho-Histone H3 antibodies (Hendzel *et al*, 1997), however, it is not feasible to distinguish between mitosis and cytokinesis cells with those (Karayel *et al*, 2018). Phospho-S34 Keratin would serve as a great biochemical biomarker to examine cytokinesis cells in the population. Given the fact that Keratin-8 is a widely used tumor diagnostic biomarker in epithelial malignancies (Karantza, 2011), anti-phospho-S34 Keratin antibodies would have great value in assessing cell cycle progression in cancer cells and monitoring the response of anti-mitotic cancer chemotherapy.

Importantly, we observed that Aurora B kinase and Keratin 8 interact during mitosis and cytokinesis. Our findings suggest that phosphorylation of Keratin 8 by Aurora B kinase facilitates this interaction. The necessity of Aurora B-dependent Keratin phosphorylation for the constriction of the cleavage furrow and Keratin 8's role in targeting Aurora B to the chromosomes and midzone suggest their functional interaction. By using CRISPR/Cas9-mediated reverse genetics, we showed that Keratin 8 knockout HeLa cells had a significantly higher rate of chromosome congression, chromosome segregation and cytokinesis defects. Those defects are likely due to impaired localization of Aurora B which perturbs error-correction and abscission checkpoint processes (Salimian *et al*, 2011; Steigemann *et al.*, 2009). How the downstream components of Aurora B kinase at the kinetochores and midzones are affected in Keratin 8 knockout cells remains to be determined. On the other hand, expression of non-phosphorylatable Keratin 8 mutation in knockout cells causes a much stronger cytokinesis phenotype than K8 KO which is likely due to insoluble Keratins at the cleavage furrow.

Unlike Aurora B kinase, Keratin 8 is only expressed in epithelial cells, therefore their functional dependency should be cell type and differentiation dependent. Keratin-8 may target Aurora B to the chromosome and midzone to facilitate its extra function of Keratin segregation in epithelial lineages. More work is required to decipher the molecular details of Keratin dependent function of Aurora B. It will be important to examine the interaction between Aurora B and different phospho-proteoforms of Keratin 8 at different mitotic stages by in situ proximity ligation assay and determine their functional relevance. Overall, our study demonstrates a functional interaction between Aurora B and Keratin 8 for successful cytokinesis in Keratin-expressing cells which provides an insight into the mechanism of cell type-specific pathways during cytokinesis.

Materials and Methods

Antibodies

The following antibodies were used; mouse monoclonal α-tubulin DM1A (Cell Signaling 3873S, Western blotting 1:1000, immunofluorescence microscopy 1:1000), mouse monoclonal Keratin 8 (Santa Cruz, sc-8020, Western blotting 1:1000, immunofluorescence microscopy 1:1000), Rabbit Polo Kinase (home-made) (Immunofluorescence microscopy 1:1000)), mouse monoclonal Aurora B (Abcam, ab3609, Western blotting 1:300, Immunofluorescence microscopy 1:300), rabbit polyclonal INCENP (Bethyl Laboratories, IHC-00060, Immunofluorescence microscopy 1:250), rabbit polyclonal INCENP (Abcam, ab12183, Western blotting 1:2500).

For generating antibodies against phospho S34 Keratin 8 (produced by Davids Biotechnology), rabbits were immunized with the KLH conjugated phospho-peptide five times. After antibody production the serum is affinity purified with the phospho-peptides. To get rid of antibodies recognizing the non-phosphopeptides, the affinity purified serum is depleted with a non-phosphopeptide depletion matrix.

Plasmids and Cloning

GFP tagged WT Keratin 8 in pEGFP-N3 (Addgene 6080) was kindly provided by Dr. Milind Vaidya (ACTREC). S13A, S34-37A Keratin 8, S21-22A Keratin 8, S39A Keratin 8, S43-44A Keratin 8, S104A Keratin 8, S258A Keratin 8, S330A Keratin 8, S410A Keratin 8, S477-478A Keratin 8 and S21-22-24-26A Keratin 8 mutant constructs were cloned into pEGFP-N3 vector by site-directed mutagenesis using WT Keratin 8:GFP. Wild type Keratin 8 was cloned into pGEX-6p-1 (Addgene) (WT-K8-GST) for in vitro assays.

Cell Culture and Synchronization

HeLa S3 cells were routinely cultured in Dulbecco's modified Eagle's medium (DMEM) (Lonza, BE12-741F) containing 10 % Fetal Bovine Serum (FBS), 100 unit/ml Penicillin and 100 µg/ml Streptomycin (Lonza, DE17-602E) at 37°C and 5% CO2. To synchronize the cells in interphase, cells were incubated with DMEM including 2 mM Thymidine (Santa Cruz, 296542A) for 20 hours, then released into fresh DMEM for 8 hours. Cells were incubated with 2 mM Thymidine for another 17 hours. To arrest cells at prometaphase, cells were incubated in DMEM including 30 nM Nocodazole (Calbiochem, 487928) for 5 hours. Cells were harvested or fixed at the end of one hour release from nocodazole to collect cytokinesis cells. To induce Aurora B inhibition at cytokinesis, cells were treated with 1 µM AZD1152 or 0.5 µM VX680 Aurora B inhibitors for 30 minutes.

CRISPR/Cas9 mediated Keratin 8 Knockout

Targeting guide with sequence 5' CGAGGAGCTGATGCGGGAA 3' and non-targeting guide with sequence 5'-ACGGAGGCTAAGCGTCGCAA-3' were cloned into pLenti CRISPRv2 using BsmBI restriction digestion of backbone using protocol from Zhang lab. HeLa S3 cells were transiently transfected with plentiCRISPRv2 plasmid containing Keratin 8 guide and non-targeting control by using Lipofectamine. Transfected cells were selected with puromycin. Serial dilution was used to prepare monoclonal cells. Loss of Keratin 8 expression in HeLa cells were detected by using immunoblotting.

Pulldown of Aurora B-GFP

Aurora B-GFP expressing cells were grown in 40% confluency and synchronized in interphase by double Thymidine Block and in mitosis by using S-trityl-L-cysteine (STC; Sigma-Aldrich) (Uretmen Kagiali *et al*, 2020). Cell pellets were lysed in l ice-cold lysis buffer (20mM Tris-CL pH7.4, 150mM NaCl, 1mM MgCl2, 10%Glycerol, 0.5mM EDTA, 10mM NaF, 0.5%NP-40, 1mM beta- glycerolphosphate, 1mM sodium pyrophosphate, 1mM sodium orthovanadate, 1mM DTT, EDTA free protease inhibitor (Pierce, 88266,) by pipetting and passing through 25-gauge needle. Cell lysates were centrifuged at 14000 rpm for 15 min at +4°C. Dilution buffer (20mM Tris-CL pH7.4, 150mM NaCl, 1mM MgCl2, 10%Glycerol, 0.5mM EDTA, 10mM NaF) was added to the supernatant in 2:3 proportions. GFP-Trap®_A (Chromotek, gta-20) was used for pulling down Aurora B-GFP. The diluted lysate was mixed with the beads and rotated for 3 hours at 4°C. After washing the beads with dilution buffer, for elution, beads were re-suspended in 2X Laemmli Sample Buffer (4% (w/v) SDS, 20% Glycerol, 120mM Tris-Cl (pH 6.8), 0.02% (w/v) bromophenol blue, 100mM DTT) and boiled for 10 min at 95°C and SDS-PAGE and Western Blotting was performed.

Transfection

WT-K8-GFP and 5XA-K8-GFP vectors were transfected to HeLa S3 cells with Lipofectamine 2000 by following the manufacturer's instructions for immunostaining and live-cell imaging experiments. HeLa S3 cells were transfected with vectors 8-24 hours before thymidine block. 300-1500 ng DNA was incubated with 1-5 µl Lipofectamine 2000 in 150 µl Optimem (Thermo Fisher, 31985047) for 10 minutes at room temperature and then given to cells. The media was changed 8-10 hours after transfection.

Immunofluorescence

Cells were grown on coverslips and fixed with 3% PFA for 15 min at 37°C. Fixed coverslips were washed with PBS-0.1% Triton-X (PBS-Tx) and incubated with blocking solution (2% BSA in PBS-Tx) for overnight at 4°C or 30 minutes at room temperature. Incubation of primary antibody in 2% BSA in PBS-Tx was

done at 4°C for overnight or at room temperature for 2 hours. Secondary antibody in 2% BSA in PBS-Tx was incubated at room temperature for 1 hours. Cell nuclei staining was done with 1 µg/ml DAPI in 2% BSA, PBS-Tx for 10 minutes at room temperature.

Microscopy, Image Analysis and Statistical Analysis

Immunofluorescence intensities were quantified using ImageJ and FiJi software (Wayne Rasband, NIH). Briefly, RGB values of different spots at metaphase chromosome or on cleavage furrow were measured by keeping the area constant and an average of these values taken. The same process was applied to random spots on the body of the cell and the fluorescence intensities were normalized by dividing or subtracting the fluorescence intensity of the cell body.

For microscopy imaging, Leica DMi8/SP8 TCS-DLS, Leica DMi8 wide-field microscope or Nikon 90i Confocal Microscope using LAS X Software and NIS-Element Imaging software and Nikon Eclipse APO λ 100X/1.40 Oil objective lens were used. Graphs were plotted by GraphPad Prism 8.

Recombinant protein expression and purification

WT-K8-GST vector was transformed into Escherichia coli (*E. coli*) BL21 competent cells by following the standard transformation protocol. A single colony was chosen and grown in 100 µg/ml Ampicillin LB at 37 °C until its OD600 reached to 0.5. Then bacteria were induced with 1 mM Isopropyl β-D-1-thiogalactopyranoside (IPTG). The recombinant protein was isolated from inclusion bodies. Briefly, bacteria was pelleted and lysed in a buffer containing 100 mM TrisCl pH 8, 5mM EDTA, 5mM DTT and 1X Protease Inhibitor (Roche, *11836170001*) using a sonicator. The suspension was centrifuged at 13,500 rpm at 4°C for 1 hour. Pellet was re-suspended in a wash buffer (50 mM TrisCl pH 8, 10 mM EDTA, 5 mM DTT, 1 M NaCl, 1% NP40). After homogenization of the pellet it was sonicated, this step was repeated one more time. After the washing steps, the pellet was extracted with extraction buffer (8 M Urea, 5 mM DTT, 2 mM EDTA, 10 mM TrisCl pH 8) and homogenized with a tissue grid homogenizer. The suspension was pelleted again, and the supernatant was used for protein purification. To refold Keratin 8:GST, the supernatant was dialyzed with dialysis buffer (25 mM Hepes pH 7.4, 100 mM KCl, 5mM MgCl2, 0.5 mM EGTA). The Glutathione beads were incubated with the supernatant overnight. The beads were washed with a wash buffer (25 mM Hepes, 150 mM KCl, 5mM MgCl2, 0.5 mM EGTA, 1 mM DTT, 0.01% NP40) at 4°C twice. Harsh wash buffer (25 mM Hepes, 600 mM KCl, 5mM MgCl2, 0.5 mM EGTA, 1 mM DTT, 0.01% NP40) was used for the third wash. WT-GST-K8 was eluted in a buffer containing 100 mM TrisCl pH 8.0, fresh 10 mM Reduced Glutathione and 1mM DTT.

***In vitro* kinase assay and Mass Spectrometry**

Isolated WT-K8-GST was incubated with purified Aurora B complex, Aurora B and INCENP fragments were co-expressed from bicistronic vector pGEX-2rbs with GST-tag at the N-terminus of Aurora B. Aurora B complex was purified with GST sepharose and eluted from beads by cleaving the GST-tag by PreScission protease in a buffer including 50 mM Tris pH 7.5, 150 mM NaCl, 1 mM EDTA, 1 mM DTT, 10 µg/ml leupeptin and 10 µg/ml pepstain. Purified Aurora B complex was gift from Dr. Masanori Mishima (University of Warwick). For in vitro kinase assay, 25 µg WT-K8-GST and 0.75 µg Aurora B complex were incubated in 100 µl kinase reaction buffer including 20 mM PIPES pH 7, 2 mM $MgCl_2$, 2 mM EGTA, 100 mM NaCl and 0.2 mM ATP at 30°C for 40 minutes. Kinase reaction was dissolved in 50 µl 3X SDS Blue Loading Buffer supplemented with 100 mM Dithiothreitol (DTT) by boiling it at 85°C for 10 minutes. After alkylation with 100 mM IA (I6125, Sigma Aldrich), the samples were loaded into 12% Tris-Glycine Precast Gels (Pierce, 25247) and stained with Page Blue Protein Staining (Thermo Fisher Scientific, 24620). The band corresponding to Keratin 8:GST (66-81 kDa) was cut and after the washing steps, the gel plugs were digested by using 1:50 (Trypsin: Protein amount ratio) Sequencing Grade

Modified Trypsin (Promega) at 37 °C overnight. Digests were desalted by Stage Tipping using Empore C18 47mm disks and resuspended in 5% FA and 5% ACN for LC-MS/MS analysis.

Mass Spectrometry Data Acquisitions and Processing

The peptides were subjected to a reversed-phase Nano LC-MS/MS (EASY-nLC, Thermo) connected to a Q Exactive quadrupole Orbitrap mass spectrometer (Thermo Fisher Scientific, Bremen). The peptides in the fractions were directly loaded onto an in-house packed 100 µm i.d. × 17 cm C18 column (Reprosil-Gold C18, 5 µm, 200Å, Dr. Maisch). Survey spectra were acquired on the Orbitrap with the resolution of 70,000 and for MS2 resolution 17,500. Raw data files were processed with Protein Discoverer (version 1.4 Thermo Scientific) and MaxQuant (version 1.5.2.8) for protein identification. The raw data was searched against database including Keratin 8:GST sequence. For the PRM analysis an inclusion lists were prepared and the samples were analysed with a 60 min linear gradient the following MS parameters: Dynamic exclusion 10 ppm, MS2 resolution 35.000, AGC target 2e5, isolation window 1.2 m/z, nce 28. The transition lists were created in Skyline v3.1 software (MacCoss Lab) with the following transition settings: precursor charges 2,3,4,5; ion charges 1,2 and eight product ions (MacLean *et al*, 2010). MS and MS/MS mass accuracy was set to 10 ppm.

Acknowledgement

We thank Dr. Milind Vaidya from ACTRECT for providing WT K8-GFP vector. We thank Dr. Masanori Mishima from Warwick University for supplying purified active Aurora B; Venkatesha Basrur and Dattatreya Mellacheruvu from the Department of Pathology Michigan University for their help with the PRM experiment; Gürkan Mollaoğlu, M. Göksu Özlü and Merve Yiğin from Koc University for their helps in the experiments. Artür Manukyan from Max Delbrück Center for his help with statistical analysis. BH was supported by a scholarship from the TUBITAK-2211E program. This work is also supported by TUBITAK #118Z832.

Author Contributions

NO and TJM conceived the project and NO, BH designed experiments. BH prepared biological samples, performed all cell biology, cloning, microscopy imaging experiments, analyzed the data and prepared the figures. OK analyzed microscopy images and performed statistical analysis. MHQ prepared HeLa S3 K8 KO cell line. AN and NO performed PRM experiment and MS and Skyline analysis. BH, TJM and NO wrote the manuscript. NO supervised the project.

Conflict of interest

N.O. and B.H. are inventors on a pending patent application from Koc University, application number 2021/009156.

Figure Legends

Figure 1. Keratin 8 knockout causes chromosome segregation and cytokinesis defects.

a. Representative images from live imaging of dividing HeLa cells (Videos S1-S3) expressing H2B-mcherry (red) in control, K8 Knockout (K8 KO) and K8-GFP (green) expressing rescued knockout (K8 KO+WT K8-GFP) cells. **b.** Quantification of multinucleated cells in control, K8 KO

and K8 KO HeLa cells expressing WT K8-GFP. *n>500* cells for each group in at least two independent experiments. Cochran-Mantel-Haenszel test (CMH) was performed. Error bars represent standard deviations (SD). **** p<0.001 **c.** Representative immunofluorescence images of metaphase cells in control, K8 KO and K8 KO+WT K8-GFP HeLa cells. Misaligned chromosomes in K8 KO cells are labeled with arrows. **d.** Quantification of percentages of cells with misaligned chromosomes at metaphase in control, K8 KO and K8 KO HeLa cells expressing WT K8-GFP. *n*=33 cells for control, *n*=35 cells for K8 KO and *n*=30 cells for K8 KO+WT K8-GFP were quantified. Cochran-Mantel-Haenszel test was performed. ** p<0.001, ns, nonsignificant. **e.** Representative immunofluorescence images of anaphase control and K8 KO HeLa cells. Abnormal chromosome segregation defects (lagging chromosome and chromosome bridge in cytokinesis) are shown in K8 KO cells. **f.** Quantification of percentages of cells with abnormal chromosome segregation in control, K8 KO and K8 KO HeLa cells expressing WT K8-GFP. *n*=123 cells for control, *n*=123 cells for K8 KO and *n*=48 cells for K8 KO+WT K8-GFP were quantified. Cochran-Mantel-Haenszel test was performed. **** p<0.001 **g.** Representative images from control or K8 KO HeLa cells live imaging (Videos 6-7) expressing Aurora B-GFP (green) H2B-mcherry (red). **h.** Quantification of the Aurora B fluorescence intensity by measuring mean intensity ratio of cleavage furrow to cytoplasm in control and K8 KO Hela cells. *n*= 16 cells for control and *n*= 18 cells for K8 KO HeLa cells were quantified. Mann Whitney U test was performed. Box-and-whisker plot represents min to max value with the mean value. **p<0.01. Scale bars, 10 µm

Figure 2. Mapping Aurora B kinase-dependent phosphorylation sites in Keratin 8 by *in vitro* kinase assay

a. Cartoon illustration depicts the experimental workflow of *in vitro* kinase assay to detect Aurora B phosphorylation sites of Keratin 8. **b.** Parallel Reaction Monitoring-Mass Spectrometry (PRM-MS) analysis of *in vitro* phosphorylation of S34 Keratin 8 by Aurora B. The peak area quantification of the nonphospho (ISSSSFSR) and phosphoS34 (IpSSSSFSR) of Keratin 8 with Aurora B (+Aurora B) and without Aurora B (- Aurora B) conditions. Each graph shows one peptide and the colored peaks show the transitions of the non-phosphopeptide (top) and phosphopeptide (bottom) **c.** The map of Aurora B dependent K8 phosphorylation sites detected by *in vitro* kinase assay. Yellow, phosphorylated Serine or Threonine residues on the head, road or tail domains of Keratin 8.

Figure 3. Non-phosphorylatable Keratin 8 mutation causes persistent Keratin 8 bundles as the cleavage furrow ingress.

a. Quantification of percentage of multinucleated cells in control, K8 KO, K8 KO HeLa cells expressing WT K8-GFP, S13,34-35A K8-GFP, S13,36-37A K8-GFP, S13,34-37A K8-GFP, S13 K8-GFP and S3435D K8-GFP. *n>350* cells for each group in at least two independent experiments. Cochran-Mantel-Haenszel test was performed. Error bars represent standard deviations (SD). * p<0.05, **** p<0.001, ns, nonsignificant **b.** Immunofluorescence staining of K8-GFP expressing cells against anti-Aurora B (red) antibodies and DAPI (blue) in control (WT K8-GFP) and mutant (S13,34-37A K8-GFP) HeLa cells. **c.** Quantification of WT K8-GFP and mutant S13,34-37A K8-GFP localization at the cleavage furrow in HeLa cells. K8-GFP intensities at the

cleavage furrow were measured and normalized to cytosolic K8-GFP intensities. *n=14 cells for* HeLa cells expressing WT K8-GFP and *n*=13 cells for HeLa cells expressing S13,34-37A K8-GFP were measured. Unpaired two-tailed *t* test was performed. Data represent SD. * p<0.05. **d.** Representative images from live imaging of cell division in K8 KO HeLa cells expressing WT K8-GFP and S13,34-37A K8-GFP (Videos S8,S9). **e.** Immunofluorescence staining for Keratin 8 (green), INCENP (red) and DAPI (blue) in control and HeLa cells treated with 1 µM AZD1152 or 0.5 VX680 µM after thirty minutes of nocodazole release. **f.** Quantification of Keratin 8 localization at the cleavage furrow in control *(n=65)*, 1 µM AZD1152 *(n=48)* or 0.5 VX680 µM *(n=57)* treated HeLa cells. One-way ANOVA with Dunnett's post hoc test was performed. **** p<0.001. Data represents mean ± SEM (Standard Error Mean). Scale bars, 10 µm

Figure 4. Phosphomimetic mutant of Keratin 8 leads to speckled Keratins

a. Representative images of phosphomimetic mutant Keratin 8 localization throughout the cell division. Still images of time-lapse movies were showed in K8 KO HeLa cells expressing mcherry-H2B and WT K8-GFP, S13,34-37A K8-GFP and S34-35D K8-GFP (Videos S13-S15 respectively). **b.** Quantification of speckled keratins in dividing K8 KO HeLa cells expressing WT K8-GFP, S13,34-37A K8-GFP and S34-35D K8-GFP. *n>15* cells for each group in at least two independent experiments. Cochran-Mantel-Haenszel test was performed. **** p<0.001, ns, nonsignificant. Scale bars, 10 µm

Figure 5. Aurora B dependent Keratin 8 S34 phosphorylation decorates cleavage furrow

a. Representative images of Keratin 8 S34 phosphorylation at the cleavage furrow. Interphase, mitosis and cytokinesis Hela cells were immunostained against endogenous Keratin 8 (green), Keratin 8 phospho S34 (red) and DNA (DAPI, blue). **b.** Representative images of HeLa cells after Aurora B inhibition. Control, 1 µM AZD1152 or 0.5 VX680 µM treated cells were immunostained against Aurora B (green), Keratin 8 phospho S34 (red) and DNA (DAPI, blue). **c.** Quantification of Keratin 8 phospho S34 fluorescence intensity at the cleavage furrow in control, 1 µM AZD1152 or 0.5 VX680 µM treated HeLa cells. *n*=11 cells for control, *n*=9 cells for 1 µM AZD1152 treated and *n*=8 cells for 0.5 VX680 µM treated cells were quantified. One-way ANOVA with Dunnett's post hoc test was performed. **** p<0.001. Data represent mean ± SEM (Standard Error Mean). Scale bars, 10 µm

Figure 6. Keratin 8 targets Aurora B kinase to the chromosomes and midzone

a. GFP pulldown of HeLa cells stably expressing Aurora B-GFP in bacterial artificial chromosomes (BAC). Immunoblotting of whole cell lysates (WCL), unbound (UB) and elutes (ELU) from control (Empty GFP) and Aurora B-GFP expressing interphase and mitosis cells using anti-INCENP, anti-Keratin 8, anti phospho histone H3 (S10) **b.** Representative images of Aurora B kinase localization in control, K8 KO, K8 KO HeLa cells expressing WT K8-GFP and S13,34-37A K8-GFP. Metaphase cells are immunostained against Aurora B (red) and DNA (DAPI, blue) **c.** Quantification of the mean intensity of Aurora B at the chromosome in control, K8 KO, K8 KO HeLa cells expressing WT K8-GFP, S13,34-37A K8-GFP Hela cells. *n*=43 cells for control, *n*=49 cells for K8 KO, *n*=45 cells for K8 KO+WT K8-GFP and *n*=49 cells for K8 KO + S13,34-37A K8-GFP were quantified. One-way ANOVA with Dunnett's post hoc test was performed. Box-and-whisker plot represents min to max value with the mean value. ****p<0.0001, ***p<0.001, n.s., no significant difference. **d.** Representative images of Aurora

B kinase localization in control, K8 KO, K8 KO HeLa cells expressing WT K8-GFP and S13,34-37A K8-GFP. Anaphase cells are immunostained against Aurora B (red) and DNA (DAPI, blue). Scale bars, 10 µm. **e.** Quantification of the mean intensity of Aurora B localization at the midzone in control, K8 KO, K8 KO HeLa cells expressing WT K8-GFP, S13,34-37A K8-GFP Hela cells. *n*=20 cells for control, *n*=20 cells for K8 KO, *n*=13 cells for K8 KO+WT K8-GFP and *n*=13 cells for K8 KO + S13,34-37A K8-GFP were quantified. One-way ANOVA with Dunnett's post hoc test was performed. Box-and-whisker plot represents min to max value with the mean value. ****p<0.0001, **p<0.01, n.s., no significant difference. Scale bars, 10 µm

Figure 7. A model describing the role of Aurora B dependent Keratin 8 phosphorylation during cytokinesis

a. At the onset of anaphase, Aurora B phosphorylates Keratin 8 at the position of S34. Phosphorylated Keratin 8 interacts with Aurora B and promotes its localization at the midzone but not Non-phosphorylatable K8 (5XA) mutant.

b. Aurora B kinase dependent phosphorylation of K8 at S34 localizes to the cleavage furrow region, phosphorylation promotes disintegration of K8 at the midzone. Inhibition of Aurora B kinase, or non-phosphorylatable Keratins result in persistent Keratin at the midzone and cytokinesis defects.

List of Supplementary items

Figure S1. The figure is related to Figure 1 . Keratin 8 knockout causes cytokinesis defects

a. Western Blotting analysis of Keratin 8 knockout by detecting Keratin 8 and Tubulin protein levels in HeLa, nontargeting gRNA and K8 gRNA treated HeLa cells. Whole cell lysates were immunoblotted with anti-α-Tubulin and anti-Keratin 8 antibodies. **b.** Immunostaining for the validation of Keratin 8 knockout colony by imaging fixed control (nontargeting gRNA) and K8 KO (K8 gRNA) HeLa cells using anti-Keratin 8 (green) and DAPI (blue). **c.** Imaging of fixed control (nontargeting gRNA) and K8 KO (K8 gRNA) HeLa cells using phalloidin (red) and DAPI (blue). Asterisks highlight multinucleated cells. **d.** Quantification of abscission time in control and K8 KO HeLa cells. 10 cells for each group were quantified busing phase images. Unpaired two-tailed *t* test was performed. Data represent SD. ** p<0.01. **e.** Representative image from live imaging of dividing HeLa cells expressing H2B-mcherry (red) and Aurora B-GFP in control and K8 Knockout (K8 KO) cells (Videos S4,S5). **f.** Quantification of the chromosomal Aurora B levels by measuring mean intensity ratio at metaphase chromosome to cytoplasm in control and K8 KO Hela cells. *n*= 6 cells for control and *n*= 8 cells for K8 KO HeLa cells were quantified. Mann Whitney U test was performed. Box-and-whisker plot represents min to max value with mean value. **p<0.01. **g**. Western Blotting analysis of Aurora B expression in control and K8 KO HeLa cells. Whole cell lysates were immunoblotted against anti-Aurora B and anti-Keratin 8 antibodies to observe endogenous Aurora B expression level. Ponceau S staining shows tubulin amount as loading control. Scale bar, 10 µm.

Figure S2. The figure is related to Figure 2. Mapping of Aurora B dependent phosphorylation of Keratin 8 *in vitro*

Parallel Reaction Monitoring-Mass Spectrometry (PRM-MS) analysis of *in vitro* phosphorylation peptides of Keratin 8 by Aurora B. The peak area quantification of the non phospho and phospho peptides of Keratin 8 with Aurora B (+Aurora B) and without Aurora B (- Aurora B) conditions. The transitions of non phospho or phospho peptide of K8 (without Aurora B (- Aurora B) and with Aurora B (+ Aurora B) (left) and their quantification (right) are shown for each peptide using Skyline. Each graph shows one peptide and the colored peaks show the transitions of the non-phosphopeptide (top) and phosphopeptide (bottom). The histogram on the right shows the total intensity of each transition (in different colors), for each transition list including m/z values.
a. non phospho ISSSSFSR and phospho ISSSpSFSR (pS37) Keratin 8
b. non phospho ASLEAAIADAEQLGELAIK and phospho ApSLEAAIADAEQLGELAIK (pS330) Keratin 8
c. non phospho MLETKWSLLQQQK and phospho MLETKWpSLLQQQK (pS124) Keratin 8
d. non phospho LESGMQNMSIHTK and phospho LEpSGMQNMSIHTK (pS404) Keratin 8
e. non phospho DGKLVSESSDVLPK and DGKLVpSESSDVLPK (pS475) Keratin 8
f. Skyline analysis compares transitions of non phospho ISSSSFSR and phospho IpSSSSFSR (pS34) peptide of K8 with the known library from in vitro assay (without Aurora B (- Aurora B) and with Aurora B (+ Aurora B).

Figure S3. The figure is related to Figure 3. Non phosphorylatable Keratin 8 mutation causes misaligned chromosomes and multinucleation.

a. Imaging of fixed control, K8 KO, K8 KO HeLa cells expressing WT K8-GFP and S13,34-37A K8-GFP (green) using phalloidin (red) and DAPI (blue). Asterisks highlight multinucleated cells. **b.** Western Blot analysis Aurora B expression in K8 KO HeLa cells expressing WT K8-GFP, S13,34-35A K8-GFP, S13,36-37A K8-GFP, S13,34-37A K8-GFP, S34-35D K8-GFP and S13 K8-GFP. Whole cell lysates were immunoblotted with anti-GFP, anti-Tubulin and anti-Aurora B antibodies. **c.** Immunofluorescence staining against α-Tubulin (red) antibody and DAPI (blue) in control, K8 KO, K8 KO HeLa cells expressing WT K8-GFP and S13,34-37A K8-GFP. Misaligned chromosomes at the metaphase stages of K8 KO cell and K8 KO HeLa cells expressing S13,34-37A K8-GFP are highlighted with arrows. **d.** Quantification of percentage of misaligned chromosomes in control, K8 KO, K8 KO+WT K8-GFP and K8 KO + S13,34-37A K8-GFP HeLa cells. n=33 cells for control, n=51 cells for K8 KO and n=43 cells for K8 KO+WT K8-GFP and n=42 cells for K8 KO + S13,34-37A K8-GFP were quantified. Cochran-Mantel-Haenszel test was performed. **** $p<0.001$, ** $p<0.01$. **e.** Representative images from live imaging of K8 KO cells expressing WT K8-GFP that are treated with DMSO (control) or Aurora B inhibitors (1 µM AZD1152 or 0.5 VX680 µM) (Videos S10-12). Scale bars, 10 µm.

Figure S4. The figure is related to Figure 4. Phospho S34 Keratin 8 antibody is not detected in Keratin 8 knockout HeLa cells

Immunofluorescence staining of Keratin 8 knockout HeLa cells at different cell cycle stages (interphase-cytokinesis) using Phospho S34 Keratin 8 (red) and Keratin 8 (green) antibodies and DAPI (blue). Scale bar, 10 µm.

Figure S5. The figure is related to Figure 4. Keratin 8 S34 phosphorylation localizes specifically to the cleavage furrow in MCF7 cells in an Aurora B dependent manner.

a. Immunofluorescence staining of MCF7 cells at different cell cycle stages (interphase, mitosis, cytokinesis) using Keratin 8 (green), Keratin 8 phospho S34 (red) antibodies and DAPI (blue). **b.** Immunofluorescence staining of control (DMSO) and Aurora B kinase inhibitor (1 µM AZD1152 or 0.5 VX680 µM) treated MCF7 cells using Keratin 8 (green), Keratin 8 phospho S34 (red) antibodies and DAPI (blue). Scale bars, 10 µm.

Figure S6. The figure is related to Figure 5. WT but not non-phosphorylatable Keratin 8 associated with Aurora B in mitosis and cytokinesis.

Co-immunoprecipitation analysis of interaction partner of Keratin 8 in **(a)** interphase, **(b)** mitosis and **(c)** cytokinesis synchronized cells using the sensitive GFP-trap approach. Western blotting analysis of whole cell lysates (WCL), unbound (UB) and elute (ELU) fractions obtained from K8 KO HeLa cells expressing stable GFP (as control), WT K8-GFP and S13,34-37A K8-GFP. anti-GFP, anti-Aurora B and anti-phospho Histone H3(S10) antibodies were used. **d.** Co-immunoprecipitation analysis of HeLa cells stable expressing GFP (control) and Aurora B-GFP in bacterial artificial chromosomes (BAC). Western blot analysis of whole cell lysates (WCL), unbound (UB) and elute (ELU) fractions were performed against anti-GFP, anti-Keratin 8 and anti-phospho Histone H3(S10) antibodies.

Video S1. Related to Figure 1. Live imaging video of HeLa nontargeting guide control cells during cell division. Phase and H2B-mcherry are merged.
Video S2. Related to Figure 1. Live imaging video of HeLa K8 KO cells during cell division. Phase and H2B-mcherry are merged.
Video S3. Related to Figure 1. Live imaging video of K8 KO HeLa cells expressing WT K8-GFP during cell division. Phase, K8-GFP and H2B-mcherry are merged.
Video S4. Related to Supplementary Figure 1. Live imaging video of HeLa nontargeting guide control cells expressing Aurora B-GFP and H2B-mcherry during cell division.
Video S5. Related to Supplementary Figure. Live imaging video of HeLa K8 KO cells expressing Aurora B-GFP and H2B-mcherry during cell division.
Video S6. Related to Figure 1. Live imaging video of control HeLa cells expressing Aurora B-GFP and H2B- mcherry.
Video S7. Related to Figure 1. Live imaging video of K8 KO HeLa cells expressing Aurora B-GFP and H2B- mcherry.
Video S8. Related to Figure 3. Live imaging video of K8 KO HeLa cells expressing WT K8-GFP during cell division. Phase and K8-GFP are merged.
Video S9. Related to Figure 3. Live imaging video of K8 KO HeLa cells expressing S13,34-37A K8-GFP during cell division. Phase and K8-GFP are merged.
Video S10. Related to Supplementary Figure 3. Live imaging video of control (DMSO treated) HeLa K8 KO expressing WT K8-GFP during cytokinesis.
Video S11. Related to Supplementary Figure 3. Live imaging video of Aurora B inhibitor (AZD1152) treated K8 KO HeLa cells expressing WT K8-GFP during cytokinesis.
Video S12. Related to Supplementary Figure 3. Live imaging video of Aurora B inhibitor (VX680) treated K8 KO HeLa cells expressing WT K8-GFP during cytokinesis.
Video S13. Related to Figure 4. Live imaging video of K8 KO HeLa cells expressing WT K8-GFP and H2B-mcherry during cell division. K8-GFP and H2B-mcherry are merged.

Video S14. Related to Figure 4. Live imaging video of K8 KO HeLa cells expressing S13,34-37A K8-GFP and H2B-mcherry during cell division. K8-GFP and H2B-mcherry are merged.
Video S15. Related to Figure 4. Live imaging video of K8 KO HeLa cells expressing S34-35D K8-GFP and H2B-mcherry during cell division. K8-GFP and H2B-mcherry are merged.

REFERENCES

Bachant JB, Klymkowsky MW (1996) A nontetrameric species is the major soluble form of keratin in Xenopus oocytes and rabbit reticulocyte lysates. *J Cell Biol* 132: 153-165

Carmena M, Wheelock M, Funabiki H, Earnshaw WC (2012) The chromosomal passenger complex (CPC): from easy rider to the godfather of mitosis. *Nat Rev Mol Cell Biol* 13: 789-803

Chen CT, Doxsey S (2009) A last-minute rescue of trapped chromatin. *Cell* 136: 397-399

Chou CF, Riopel CL, Rott LS, Omary MB (1993) A significant soluble keratin fraction in 'simple' epithelial cells. Lack of an apparent phosphorylation and glycosylation role in keratin solubility. *J Cell Sci* 105 (Pt 2): 433-444

David M, Petit D, Bertoglio J (2012) Cell cycle regulation of Rho signaling pathways. *Cell Cycle* 11: 3003-3010

Dechat T, Adam SA, Taimen P, Shimi T, Goldman RD (2010) Nuclear lamins. *Cold Spring Harb Perspect Biol* 2: a000547

Eriksson JE, He T, Trejo-Skalli AV, Harmala-Brasken AS, Hellman J, Chou YH, Goldman RD (2004) Specific in vivo phosphorylation sites determine the assembly dynamics of vimentin intermediate filaments. *J Cell Sci* 117: 919-932

Field CM, Pelletier JF, Mitchison TJ (2019) Disassembly of Actin and Keratin Networks by Aurora B Kinase at the Midplane of Cleaving Xenopus laevis Eggs. *Curr Biol* 29: 1999-2008 e1994

Gard DL (1999) Confocal microscopy and 3-D reconstruction of the cytoskeleton of Xenopus oocytes. *Microsc Res Tech* 44: 388-414

Gerace L, Blobel G (1980) The nuclear envelope lamina is reversibly depolymerized during mitosis. *Cell* 19: 277-287

Goto H, Inagaki M (2007) Production of a site- and phosphorylation state-specific antibody. *Nat Protoc* 2: 2574-2581

Goto H, Yasui Y, Kawajiri A, Nigg EA, Terada Y, Tatsuka M, Nagata K, Inagaki M (2003) Aurora-B regulates the cleavage furrow-specific vimentin phosphorylation in the cytokinetic process. *J Biol Chem* 278: 8526-8530

Hatzfeld M, Keil R, Magin TM (2017) Desmosomes and Intermediate Filaments: Their Consequences for Tissue Mechanics. *Cold Spring Harb Perspect Biol* 9

Helfand BT, Mendez MG, Murthy SN, Shumaker DK, Grin B, Mahammad S, Aebi U, Wedig T, Wu YI, Hahn KM *et al* (2011) Vimentin organization modulates the formation of lamellipodia. *Mol Biol Cell* 22: 1274-1289

Hendzel MJ, Wei Y, Mancini MA, Van Hooser A, Ranalli T, Brinkley BR, Bazett-Jones DP, Allis CD (1997) Mitosis-specific phosphorylation of histone H3 initiates primarily within pericentromeric heterochromatin during G2 and spreads in an ordered fashion coincident with mitotic chromosome condensation. *Chromosoma* 106: 348-360

Inaba H, Yamakawa D, Tomono Y, Enomoto A, Mii S, Kasahara K, Goto H, Inagaki M (2018) Regulation of keratin 5/14 intermediate filaments by CDK1, Aurora-B, and Rho-kinase. *Biochem Biophys Res Commun* 498: 544-550
Karantza V (2011) Keratins in health and cancer: more than mere epithelial cell markers. *Oncogene* 30: 127-138
Karayel O, Sanal E, Giese SH, Uretmen Kagiali ZC, Polat AN, Hu CK, Renard BY, Tuncbag N, Ozlu N (2018) Comparative phosphoproteomic analysis reveals signaling networks regulating monopolar and bipolar cytokinesis. *Sci Rep* 8: 2269
Ku NO, Toivola DM, Zhou Q, Tao GZ, Zhong B, Omary MB (2004) Studying simple epithelial keratins in cells and tissues. *Methods Cell Biol* 78: 489-517
Lane EB, Rugg EL, Navsaria H, Leigh IM, Heagerty AH, Ishida-Yamamoto A, Eady RA (1992) A mutation in the conserved helix termination peptide of keratin 5 in hereditary skin blistering. *Nature* 356: 244-246
MacLean B, Tomazela DM, Shulman N, Chambers M, Finney GL, Frewen B, Kern R, Tabb DL, Liebler DC, MacCoss MJ (2010) Skyline: an open source document editor for creating and analyzing targeted proteomics experiments. *Bioinformatics* 26: 966-968
Omary MB, Ku NO, Liao J, Price D (1998) Keratin modifications and solubility properties in epithelial cells and in vitro. *Subcell Biochem* 31: 105-140
Orr B, De Sousa F, Gomes AM, Afonso O, Ferreira LT, Figueiredo AC, Maiato H (2021) An anaphase surveillance mechanism prevents micronuclei formation from frequent chromosome segregation errors. *Cell Rep* 37: 109783
Ozlu N, Monigatti F, Renard BY, Field CM, Steen H, Mitchison TJ, Steen JJ (2010) Binding partner switching on microtubules and aurora-B in the mitosis to cytokinesis transition. *Mol Cell Proteomics* 9: 336-350
Papini D, Levasseur MD, Higgins JMG (2021) The Aurora B gradient sustains kinetochore stability in anaphase. *Cell Rep* 37: 109818
Polat AN, Karayel O, Giese SH, Harmanda B, Sanal E, Hu CK, Renard BY, Ozlu N (2015) Phosphoproteomic Analysis of Aurora Kinase Inhibition in Monopolar Cytokinesis. *J Proteome Res* 14: 4087-4098
Poser I, Sarov M, Hutchins JR, Heriche JK, Toyoda Y, Pozniakovsky A, Weigl D, Nitzsche A, Hegemann B, Bird AW *et al* (2008) BAC TransgeneOmics: a high-throughput method for exploration of protein function in mammals. *Nat Methods* 5: 409-415
Prahlad V, Yoon M, Moir RD, Vale RD, Goldman RD (1998) Rapid movements of vimentin on microtubule tracks: kinesin-dependent assembly of intermediate filament networks. *J Cell Biol* 143: 159-170
Rieder CL, Hard R (1990) Newt lung epithelial cells: cultivation, use, and advantages for biomedical research. *Int Rev Cytol* 122: 153-220
Salimian KJ, Ballister ER, Smoak EM, Wood S, Panchenko T, Lampson MA, Black BE (2011) Feedback control in sensing chromosome biorientation by the Aurora B kinase. *Curr Biol* 21: 1158-1165
Steigemann P, Gerlich DW (2009) An evolutionary conserved checkpoint controls abscission timing. *Cell Cycle* 8: 1814-1815
Steigemann P, Wurzenberger C, Schmitz MH, Held M, Guizetti J, Maar S, Gerlich DW (2009) Aurora B-mediated abscission checkpoint protects against tetraploidization. *Cell* 136: 473-484
Uretmen Kagiali ZC, Saner N, Akdag M, Sanal E, Degirmenci BS, Mollaoglu G, Ozlu N (2020) CLIC4 and CLIC1 bridge plasma membrane and cortical actin network for a successful cytokinesis. *Life Sci Alliance* 3

Virtakoivu R, Mai A, Mattila E, De Franceschi N, Imanishi SY, Corthals G, Kaukonen R, Saari M, Cheng F, Torvaldson E *et al* (2015) Vimentin-ERK Signaling Uncouples Slug Gene Regulatory Function. *Cancer Res* 75: 2349-2362

Harmanda et al. Figure 1

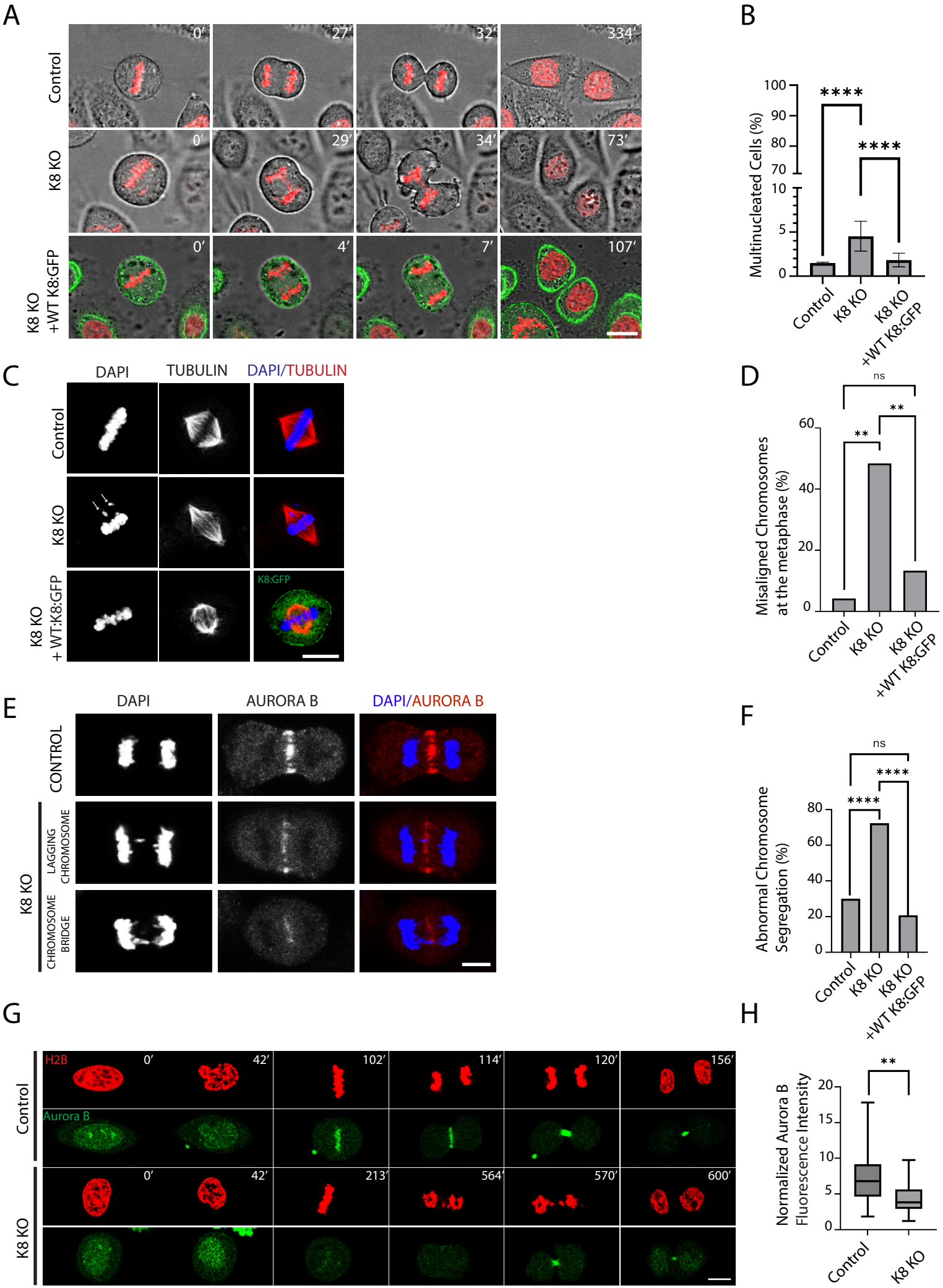

Harmanda et al. Figure 2

A

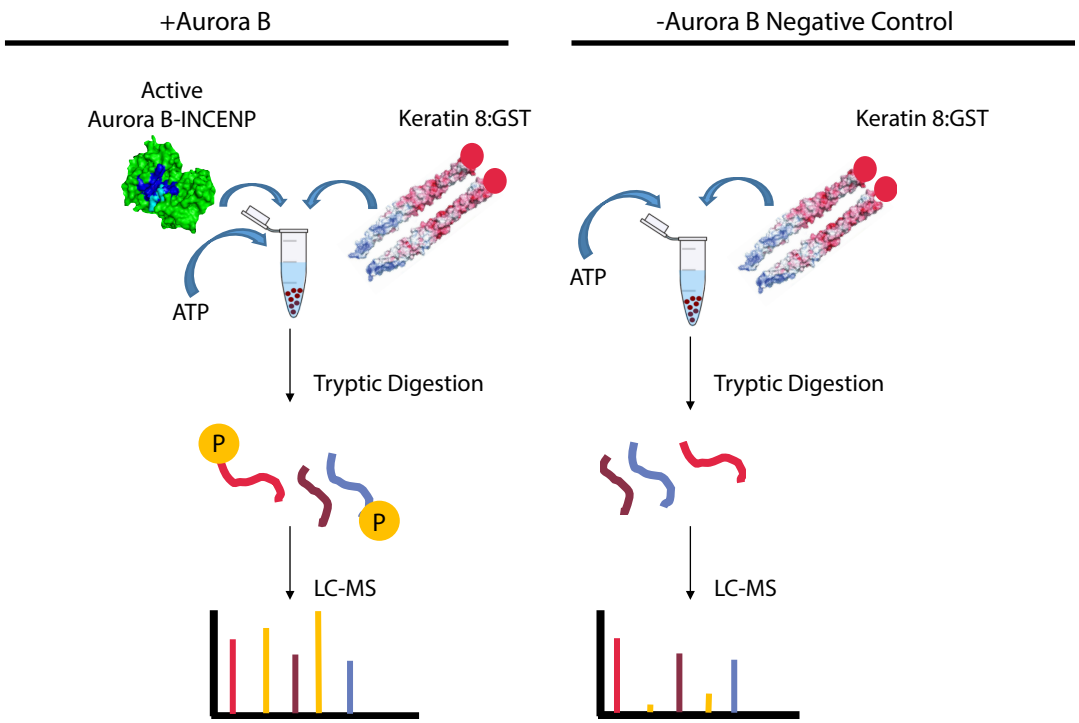

B

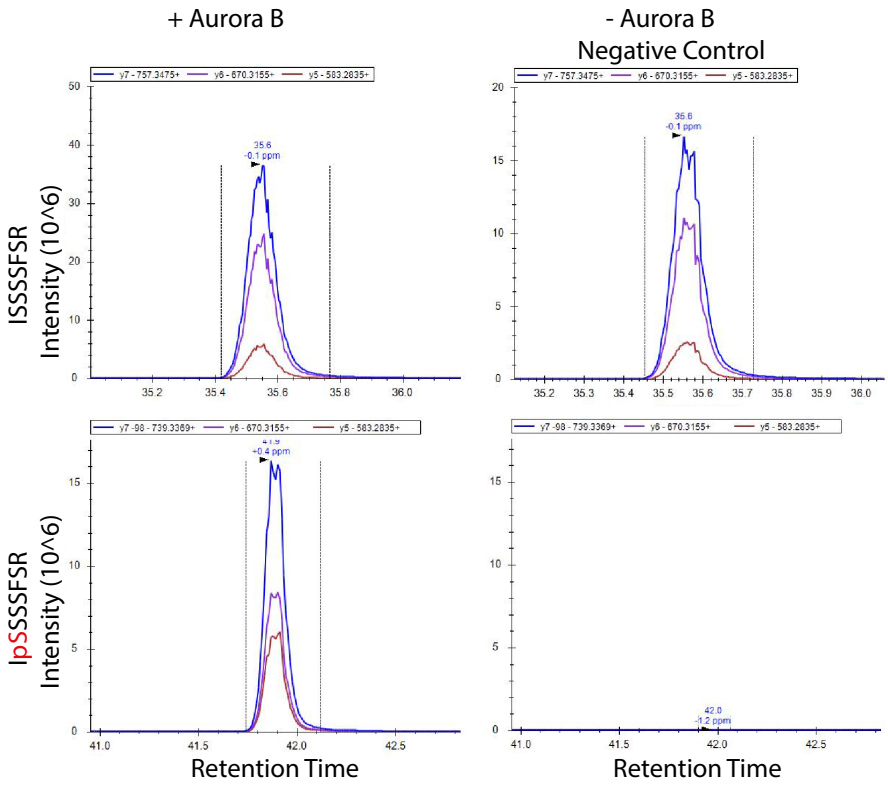

C

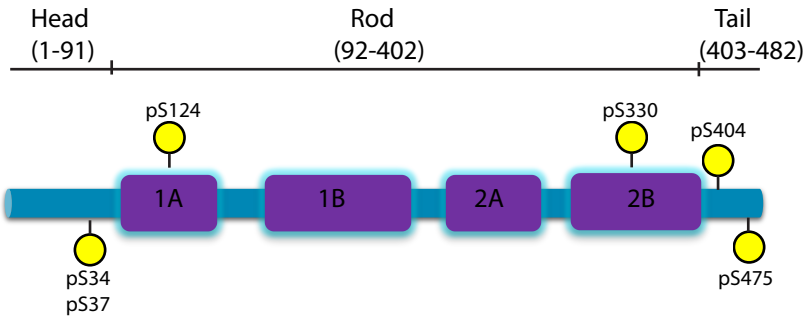

Harmanda et al. Figure 3

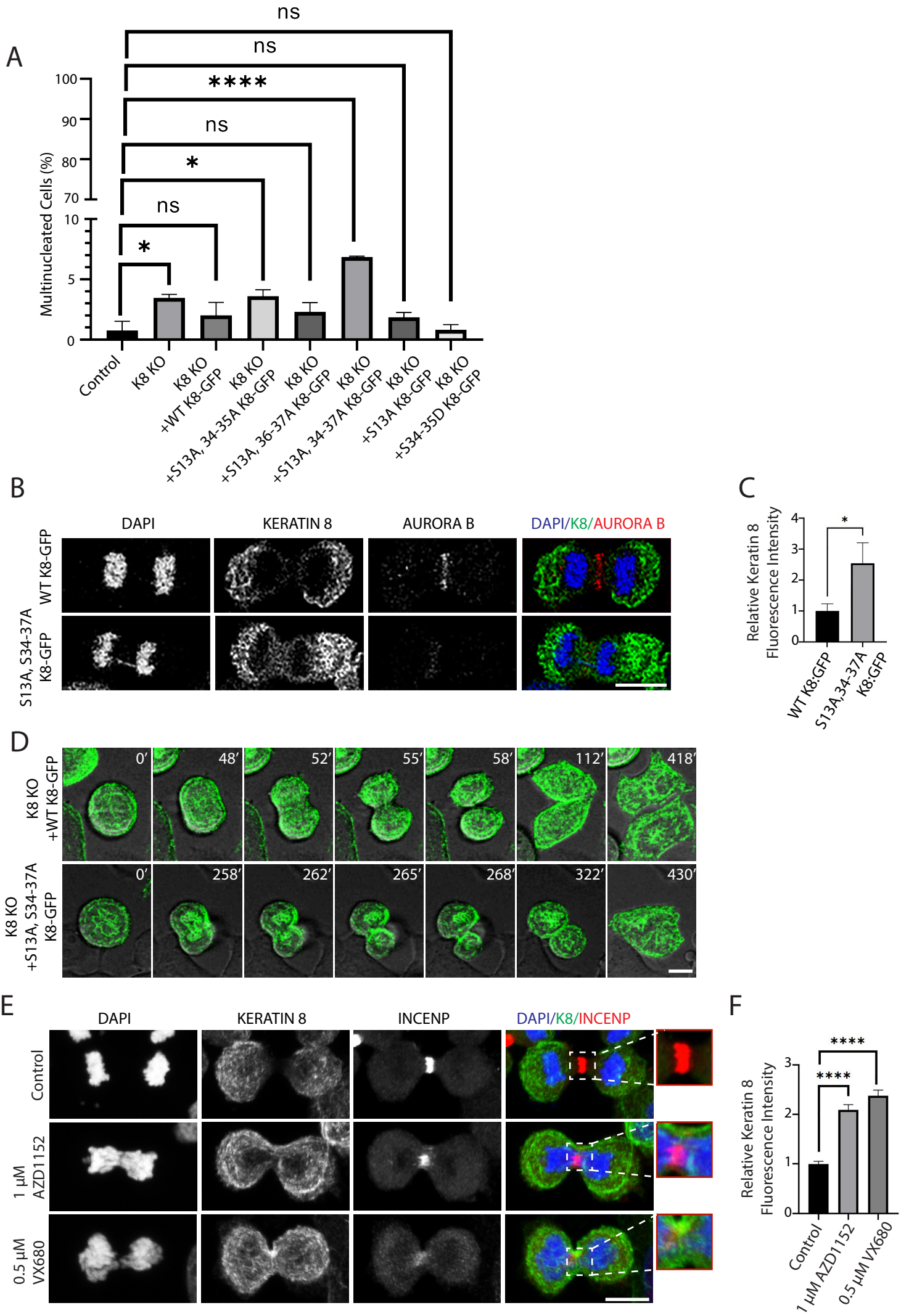

Harmanda et al. Figure 4

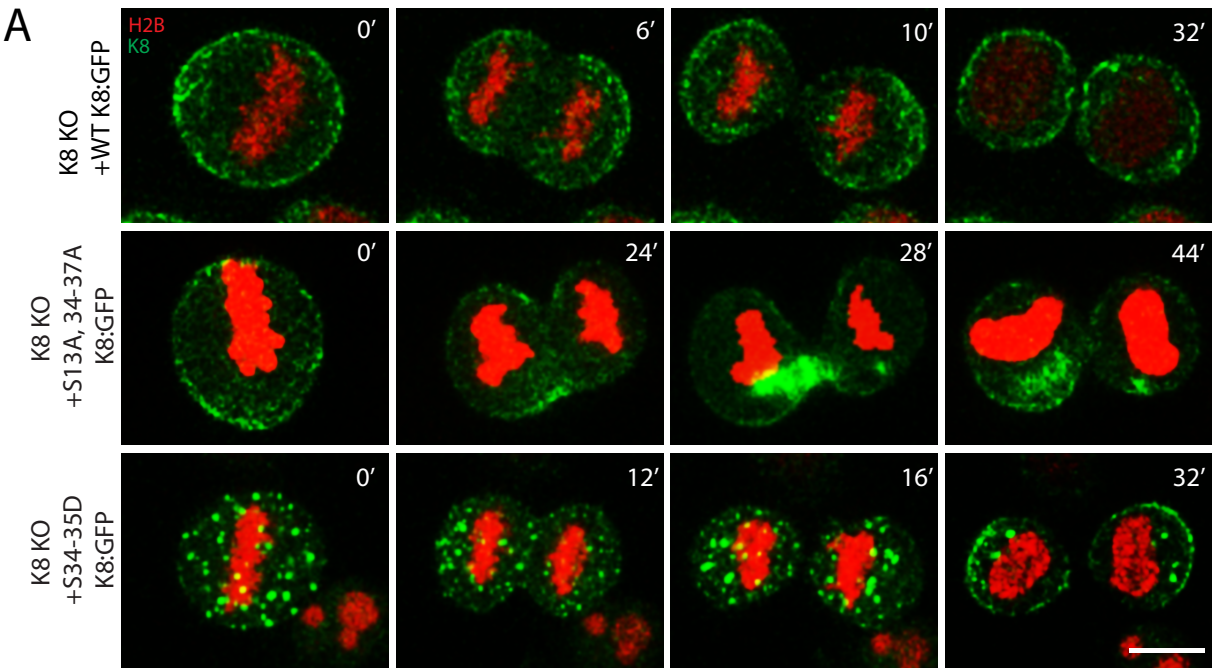

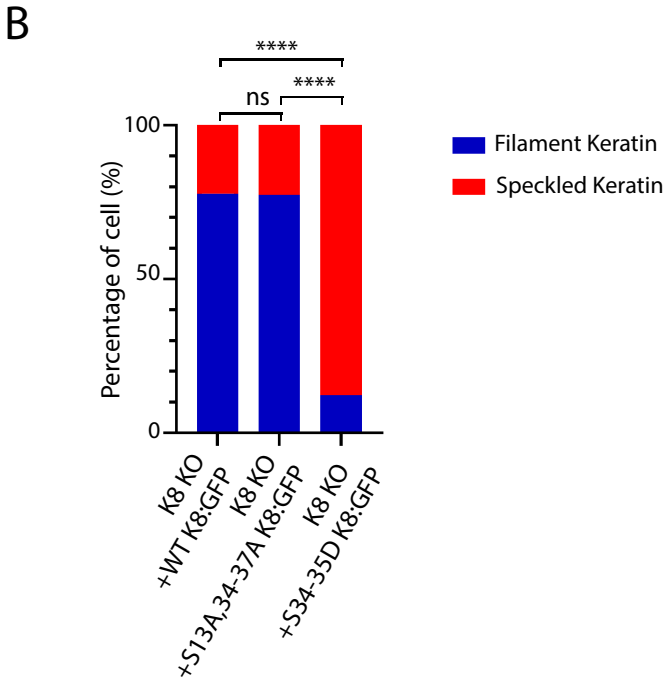

Harmanda et al. Figure 5

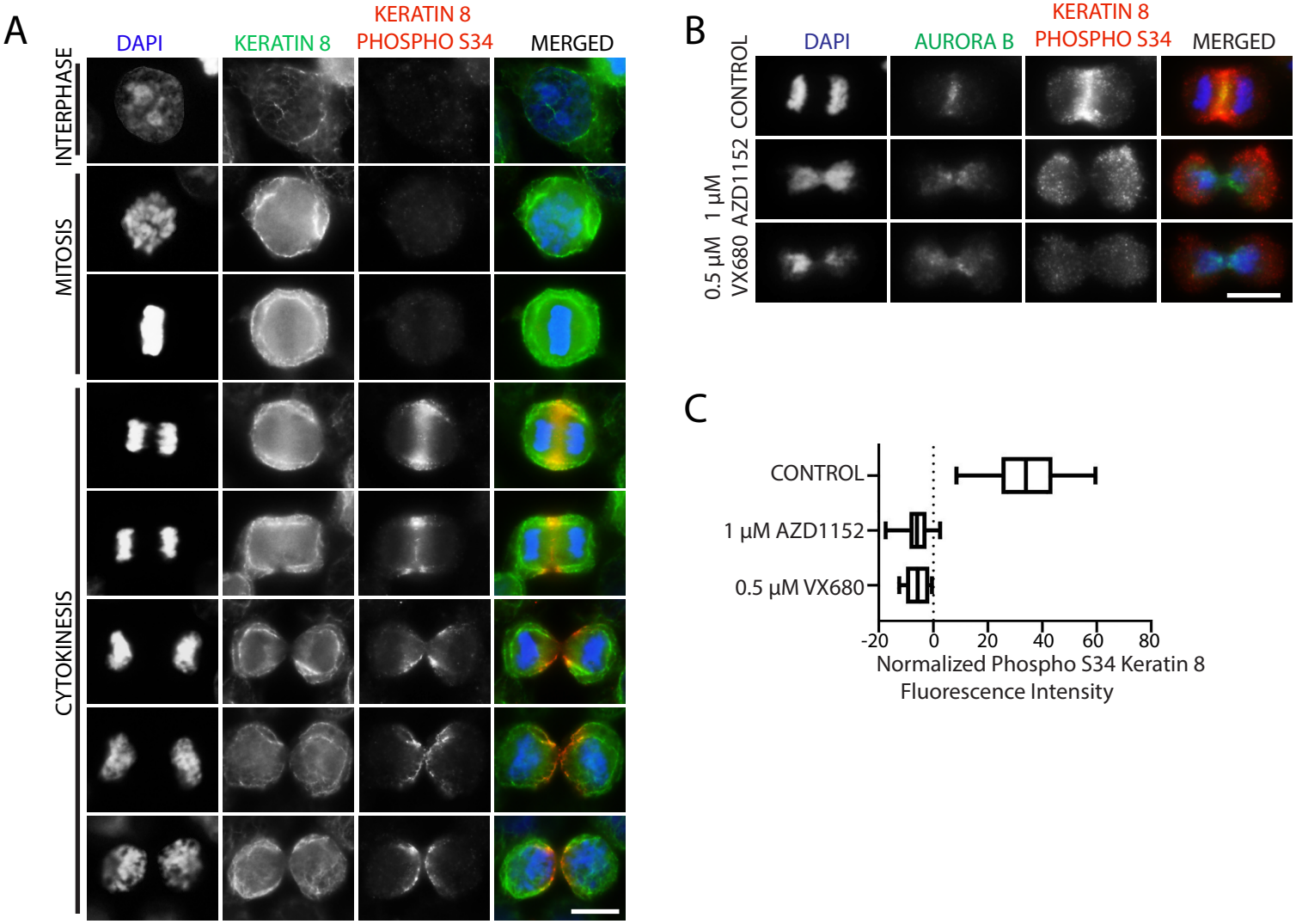

Harmanda et al. Figure 6

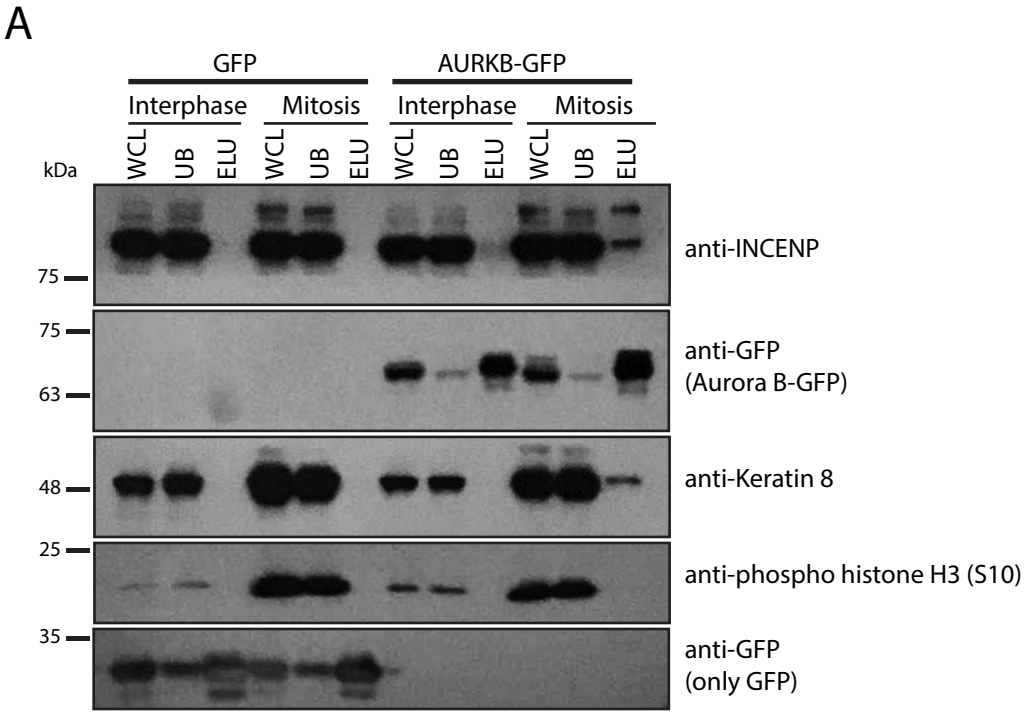

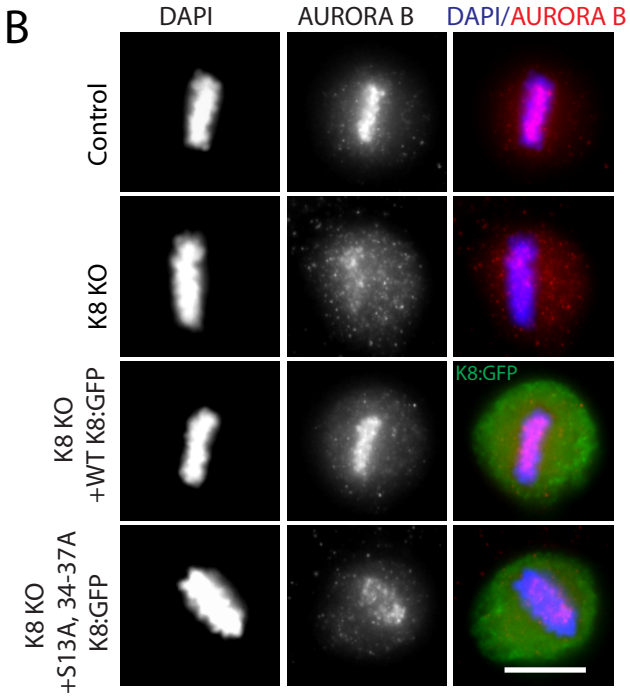

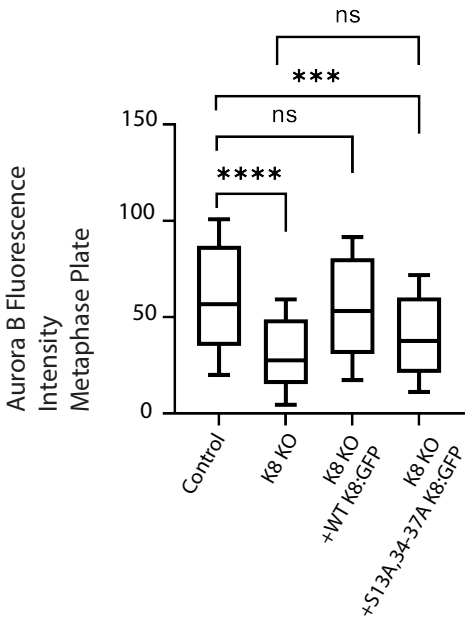

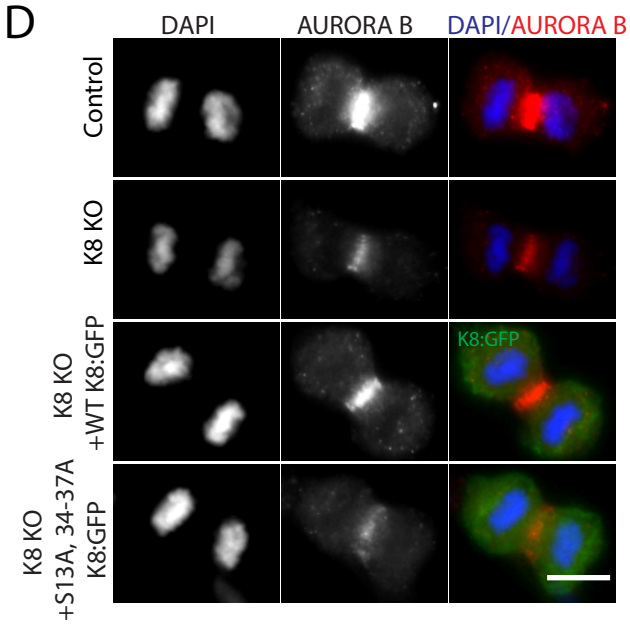

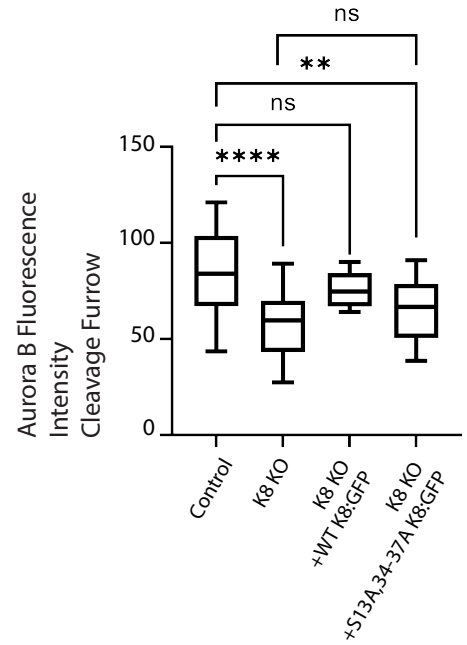
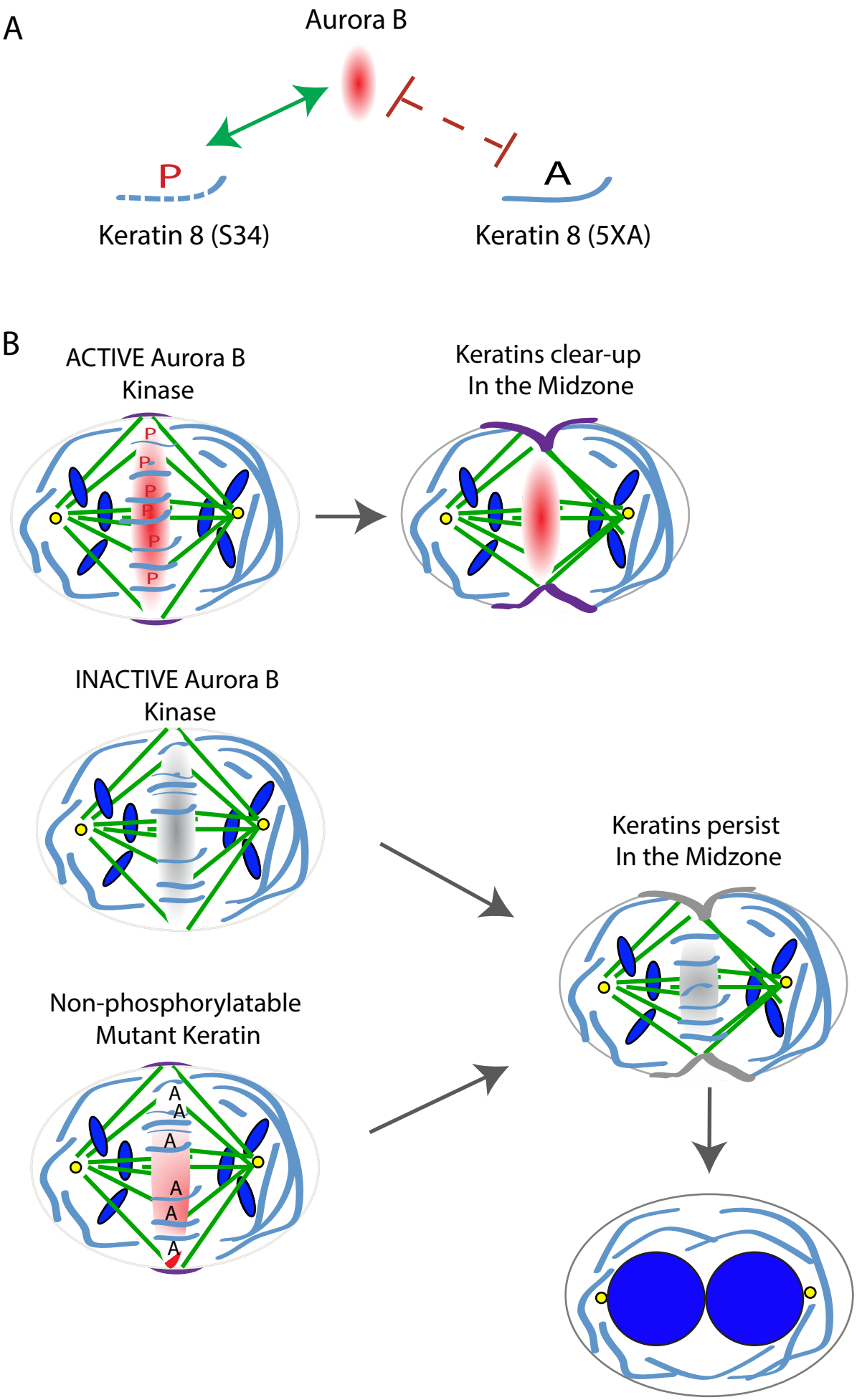
Harmanda et al. Figure 7